Characterization of atmospheric ammonia near Fort Worth, TX – Part II. Impact of ammonia on particulate matter formation

L. Gong[1], R. Lewicki[2,3], Y. J. Leong[1], B. Karakurt Cevik[1], A. P. Rutter[1,4], K. M. Shakya[1,5], R. J. Griffin[1], F. K. Tittel[2], J. H. Flynn[6], B. L. Lefer[6], E. Scheuer[7], J. E. Dibb[7], and S. Kim[8,9]

[1]Department of Civil and Environmental Engineering, Rice University, Houston, TX, USA

[2]Department of Electrical and Computer Engineering, Rice University, Houston, TX, USA

[3]Now at Sentinel Photonics, Inc., Monmouth Junction, NJ, USA

[4]Now at Sonoma Technology, Inc., Petaluma, CA, USA

[5]Now at the School of Public Health and Health Sciences, University of Massachusetts Amherst, Amherst, MA, USA

[6]Department of Earth and Atmospheric Sciences, University of Houston, Houston, TX, USA

[7]Institute for the Study of Earth, Oceans, and Space, University of New Hampshire, Durham, NH, USA

[8]Earth and Sun Systems Laboratory, Atmospheric Chemistry Division, National Center for Atmospheric Research, Boulder, CO, USA

[9]Now at Department of Earth System Science, University of California, Irvine, CA, USA

Correspondence to: R. J. Griffin (rob.griffin@rice.edu)

Abstract

Intensive measurements of gaseous and aerosol species were made at a suburban site near Fort Worth in June 2011. Inorganic aerosol components of submicron particles (PM_1) were dominated by sulfate (SO_4^{2-}) (1.25 ± 0.66 μg m^{-3}), followed by ammonium (NH_4^+) (0.44 ± 0.24 μg m^{-3}) and nitrate (NO_3^-) (0.12 ± 0.11 μg m^{-3}). Data regarding gas-phase ammonia (NH_3) and acidic trace gases such as nitric acid (HNO_3) and hydrochloric acid (HCl) were collected simultaneously. Pearson's correlation coefficients between NH_4^+, SO_4^{2-}, and NO_3^- suggest that particulate NH_4^+ mainly existed as ammonium sulfate ($(NH_4)_2SO_4$) and that ammonium nitrate (NH_4NO_3) was not formed during most of the study period, likely due to high temperatures (30.15 ± 4.12 ^oC) over the entire campaign. Ambient aerosols tended to be nearly neutral. Theoretical calculations of thermodynamic equilibrium were performed to consider the formation of NH_4NO_3 and ammonium chloride (NH_4Cl). When relative humidity (RH) was lower than deliquescence relative humidity (DRH), $P_{NH3}P_{HNO3}$ and $P_{NH3}P_{HCl}$ (i.e., partial pressure products) were smaller than the associated equilibrium constants, indicating the lack of NH_4NO_3 and NH_4Cl formation. When RH was above DRH, higher levels of NO_3^- often were observed. A strong relationship between NO_3^- and SO_4^{2-} at higher RH implies that NH_4NO_3 might be formed on the moist surface of pre-existing sulfate aerosols. In the particle mixture, $(NH_4)_2SO_4$ reduces the equilibrium constant, making the aqueous system a more favorable medium for NH_4NO_3 formation. In addition, measured particle number size distributions showed that an aerosol growth event was coincident with humid periods characterized by substantially increased concentrations of particulate NH_4^+, NO_3^-, and SO_4^{2-}. Excess NH_4^+ also was found to be correlated closely with NO_3^- during this

episode when elevated PM_1 levels imply aqueous NH_4NO_3 formation. Significant NH_3-induced formation of organic nitrogen also might have contributed to the increased particle concentration at high RH.

Keywords: ammonia, particulate matter, gas-particle partitioning, equilibrium constant

1. Introduction

Ammonia (NH_3) is recognized as an important atmospheric constituent because it actively participates in chemical reactions with acidic gaseous species such as sulfuric acid (H_2SO_4), nitric acid (HNO_3), and hydrochloric acid (HCl). This neutralization process plays a critical role in determining ambient aerosol acidity. The resulting ammonium salts largely constitute particulate matter (PM) that has strong implications for air quality, cloud formation, and human health [*Pope and Dockery*, 2006; *IPCC*, 2007]. However, spatial and temporal variations of gas-phase NH_3 are poorly understood [*Clarisse et al.*, 2009]. Global NH_3 emissions have been substantially elevated over the last several decades due to increased anthropogenic activities, especially agriculture, and the lack of regulatory controls [*Sutton et al.*, 2008]. The abundance of atmospheric NH_3 is underestimated by the current emissions inventory [*Myles*, 2009].

Ammonia measurements are notoriously difficult and are usually not included routinely in governmental air quality monitoring network sites. Measured atmospheric NH_3 levels in the Dallas-Fort Worth (DFW) area remain ambiguous, and pertinent information is very scarce in the previous studies, even comprehensive field campaigns such as the Texas Air

Quality Study. The only published literature regarding ambient NH_3 sampling in the DFW area calculated the NH_3 emission factor from oak forests at Cooper Lake State Park in Delta County and predicted that domestic sources (e.g., dogs, cats, and humans) are predominant contributors to non-industrial NH_3 emissions in Dallas County (DC) (41%) and Tarrant County (TC) (45%) of the DFW area [*Sarwar et al.*, 2005]. The National Emissions Inventory of the United States Environmental Protection Agency (U.S. EPA), by contrast, estimates that on-road gasoline light duty vehicles have the largest contribution among all source categories of NH_3 in DC (52%) and TC (46%) [*U.S. EPA*, 2008]. This prominent discrepancy underscores the paucity of sufficient experimental data. Some pioneering efforts have been made. For example, *Gong et al.* [2013a] presented relevant results from a one-month campaign and provided new insights into NH_3 sources in the DFW area.

The gas-particle partitioning and salt formation of NH_3 has been investigated recently in some urban and suburban areas throughout the world. In the South Coast Air Basin of California, *Nowak et al*. [2012] concluded based on aircraft measurements that NH_3 emitted from dairy facilities and automobiles lead to thermodynamically favorable conditions for ammonium nitrate (NH_4NO_3) formation. In the Great Lakes region, *Stanier et al*. [2012] noted that wintertime air pollution episodes were characterized by large contributions of NH_4NO_3 to PM under low temperature, high relative humidity, and air mass stagnation conditions. In Ontario, *Ellis et al*. [2011] observed that NH_3 was efficiently converted to particulate ammonium (NH_4^+) in the presence of high levels of sulfate (SO_4^{2-}), which subsequently triggered NH_3 release from the surface due to bi-directional flux. In Houston, *Gong et al*. [2013b] indicated that industrial NH_3 emissions contributed to the enhancements

in particle mass concentration and particle number concentration during summer. In Beijing, *Meng et al*. [2011] reported that NH_3 was correlated closely with NH_4^+, that NH_4^+ primarily existed as ammonium sulfate ($(NH_4)_2SO_4$) in summer, and that both $(NH_4)_2SO_4$ and NH_4NO_3 were major forms of particulate NH_4^+ in winter. In Shanghai, *Du et al*. [2010] found that NH_4NO_3 and ammonium chloride (NH_4Cl) were present in sampled $PM_{2.5}$ (d_p <2.5 μm) and PM_{10} (d_p <10 μm), indicating that NH_3 is a vital precursor of aerosol particles in the polluted atmosphere. In Barcelona, *Pandolfi et al*. [2012] attributed the low gas fraction of NH_3, defined as the molar concentration ratio of gaseous NH_3 to total NH_3 (the sum of NH_3 and NH_4^+), to significant secondary formation of sulfate, suggesting that the evolution of NH_3 concentrations is controlled by gas-particle partitioning.

However, the evaluation of the impact of NH_3 on local and regional air quality with respect to PM formation in the DFW area is far from complete. In this work conducted near Fort Worth, the mixing ratios of NH_3 and primary acidic trace gases were fully examined [*Gong et al.,* 2013a], the mass concentrations of aerosol components such as NH_4^+ in submicron particles (PM_1) were systematically explored, and the size distributions of fine particles were simultaneously determined, consequently improving the present understanding of the gas-particle partitioning of NH_3 in the study region.

2. Experimental Methods

Atmospheric NH_3 measurements were performed using a 10.4-μm external cavity quantum cascade laser-based sensor employing conventional photo-acoustic spectroscopy. Detailed information about the NH_3 instrument can be found in *Gong et al*. [2011]. In

contrast to traditional bulk denuder techniques for NH_3 sampling, which often suffer from low time resolution and human-induced contamination during sample transport, this laser-based sensor is designed to target only NH_3 gas molecules with high sensitivity (detection limit of 0.7 parts per billion (ppb)) and high selectivity (minimized interferences by other gaseous species), thereby achieving real-time gas-phase NH_3 detection without disturbances from particulate NH_4^+. Relevant measurement techniques for other gaseous species (e.g., carbon monoxide (CO), sulfur dioxide (SO_2), nitrogen oxides (NO_x), total reactive nitrogen species (NO_y), HNO_3, soluble chloride (presumably HCl), and volatile organic compounds (VOCs)) and meteorological parameters (e.g., temperature, relative humidity (RH), wind direction, and wind speed) are summarized in *Gong et al*. [2013a]. Mass concentration and chemical composition (e.g., NH_4^+, SO_4^{2-}, and nitrate (NO_3^-)) of PM_1 were measured using an Aerodyne High-Resolution Time-of-Flight Aerosol Mass Spectrometer (HR-ToF-AMS) at 15-minute intervals. Black carbon (BC) data were collected using an aethalometer (Magee Scientific, Model AE51). In addition, particle number-based size distributions covering a range from 20 to 498 nm were monitored using a Scanning Electrical Mobility Spectrometer (SEMS) (BMI, Model 2002). The campaign was performed in the early summer of 2011 at the Eagle Mountain Lake continuous ambient monitoring station (CAMS 75) administrated by the Texas Commission on Environmental Quality (TCEQ) as described in *Gong et al*. [2013a].

3. Results and Discussion

3.1 Temporal and Diurnal Variations of Aerosol Species

Figure 1 shows time series of hourly-averaged HR-ToF-AMS data along with meteorological parameters during the aerosol measurements (9 June 2011 – 30 June 2011). The statistics of the dataset for aerosol components are listed in Table 1. Their mass concentrations displayed a large amount of variability. Sulfate (overall average ± one standard deviation, 1.25 ± 0.66 μg m^{-3}) accounted for 69% of total inorganic PM_1 mass, which ranged from 0.35 to 8.18 μg m^{-3} with a mean of 1.81 ± 0.94 μg m^{-3}. The highest pollution level occurred around midnight on 23 June, 2011, when the largest spike of SO_4^{2-} was observed under low wind speed conditions. Ammonium (0.44 ± 0.24 μg m^{-3}) tracked SO_4^{2-} closely, indicating that NH_4^+ was mostly formed through the neutralization of H_2SO_4 by NH_3. Nitrate (0.12 ± 0.11 μg m^{-3}) did not change significantly, except during periods when gas-phase HNO_3 also was substantially available, suggesting that NO_3^- might be formed primarily through gas-particle conversion [*Gong et al.*, 2013a]. In addition, important environmental variables for PM formation, temperature (30.15 ± 4.12 ^oC) and RH (47.17±16.84 %) were continuously recorded, and their effects are discussed in detail in the following sections. Wind mainly blew from southeast and south-southeast (70% of the time during the campaign) throughout the measurements, and wind speed (8.18 ± 1.37 m s^{-1}) reached up to 12.51 m s^{-1} in the middle of the campaign.

Figure 2 illustrates the diurnal profiles of inorganic aerosol species in PM_1 based on the HR-ToF-AMS data. The bottom whisker, box bottom, line inside the box, box top, and top whisker represent the 10th, 25th, 50th, 75th, and 90th percentiles of the data, respectively, and the continuous solid lines represent mean values. In general, it can be seen that NH_4^+ increased in the morning and evening, with a greater magnitude in the enhancement during

the later period. The behavior of SO_4^{2-} was very similar to NH_4^+, indicating the probable presence of $(NH_4)_2SO_4$ and/or NH_4HSO_4. Nitrate tended to be relatively constant, on average, between midnight and 05:00 CST, but variable from day to day. The levels decreased in the morning, while a slow but steady increase was observed after the sunset. LIDAR-measured planetary boundary layer (PBL) height (not shown here) started to increase at 07:00 CST and reached the maximum value (2000 m) around 17:00 CST, after which it rapidly decreased and remained as low as 500 m at night. It is likely that the dynamics of PBL affected the trend of aerosol species in the evening when their concentration levels rose in a developing nocturnal PBL.

3.2 Ammonium Salt Formation

Figure 3 presents scatter plots of $[NH_4^+]$ versus $[NO_3^-]$, $[SO_4^{2-}]$ (to prevent overlap in the figure, $2[SO_4^{2-}]$ is not adopted here), and $[NO_3^-] + 2[SO_4^{2-}]$ (all in units of μmol m^{-3}). The regression yields a strongly linear relationship between NH_4^+ and SO_4^{2-} with a Pearson's correlation coefficient (r) of 0.98. The slope (0.52) of the regression line implies that NH_4^+ mainly existed as $(NH_4)_2SO_4$. This is further confirmed by a mean equivalence ratio (i.e. $[NH_4^+]/2[SO_4^{2-}]$) of 0.94. By contrast, no such good relationship exists between NH_4^+ and NO_3^- (r=0.41). In addition, the near-unit slope (1.09) of the regression line between $[NH_4^+]$ and $[NO_3^-] + 2[SO_4^{2-}]$ suggests that ambient aerosols typically were nearly neutral.

In order to investigate the formation of NH_4NO_3 and NH_4Cl, theoretical calculations of thermodynamic equilibrium for the chemical reactions between NH_3 and HNO_3 or HCl were performed. When ambient RH is lower than deliquescence RH (DRH), NH_4NO_3 and NH_4Cl

are solids at equilibrium, and the equilibrium constants can be estimated empirically [*Stelson and Seinfeld*, 1982a; *Pio and Harrison*, 1987].

$$K_{NH4NO3}=\exp[84.6-24220/T-6.1\ln(T/298)] \quad (1)$$

$$K_{NH4Cl}=\exp[2.2358\ln T-2.13204*10^{4}T^{-1}+65.437516-8.167*10^{-3}T+4.64383*10^{-7}T^{2} -1.10475*10^{-10}T^{3}] \quad (2)$$

where K_i is the equilibrium constant for salt *i* and T is temperature in Kelvin.

The DRH for NH_4NO_3 and NH_4Cl can be determined as follows [*Pio and Harrison*, 1987; *Seinfeld and Pandis*, 2006]

$$(DRH)_{NH4NO3}=\exp[1.6954+723.7/T] \quad (3)$$

$$(DRH)_{NH4Cl}=137.13-0.2T \quad (4)$$

When ambient RH is higher than DRH, NH_4NO_3 and NH_4Cl take water up and exist in the aqueous phase. In this study, RH is below DRH during the majority of the measurement period. Figure 4 (a) presents the theoretically calculated equilibrium constant for solid NH_4NO_3 (solid line) based on Equation (1) and the partial pressure product $P_{NH3}P_{HNO3}$ as a function of ambient temperature under RH<DRH conditions. On the *x* axis, 1000/T values vary between 3.20 and 3.36 K^{-1}, corresponding to a range of 24.47 to 39.35 ^{o}C. The equilibrium constant is very sensitive to the ambient temperature, changing over two orders of magnitude. It is noted that $P_{NH3}P_{HNO3}$ calculated using measured mixing ratios of NH_3 and HNO_3 was always smaller than K_{NH4NO3}. Therefore, the thermodynamic condition was not favorable for NH_4NO_3 formation, and solid NH_4NO_3 is not expected to be formed. During those periods, measured NO_3^- concentrations remained relatively low and did not change significantly.

By contrast, when RH is above DRH, increased levels of NO_3^- were observed. Figure

5 illustrates this phenomenon in that NO_3^- concentrations were relatively elevated at high RH. There was a poor overall relationship (r=0.32) between NO_3^- and SO_4^{2-} during the entire study period. It is probably influenced by the frequent absence of NH_4NO_3 formation due to high temperatures and inadequate NH_3 and/or HNO_3 in the gas phase. K_{NH4NO3} decreases as aerosols deliquesce (increasing RH) and the ionic strength of NH_4NO_3 decreases [*Stelson*, 1982]. As a consequence, the abundance of NH_3 and HNO_3 in the atmosphere required for NH_4NO_3 formation decreases. The new equilibrium constant K_{NH4NO3}^* can be derived by multiplying K_{NH4NO3} by the NH_4NO_3 ionic strength fraction (Y) which is expressed by $Y=[NH_4NO_3]/([NH_4NO_3]+3[(NH_4)_2SO_4])$ [*Stelson and Seinfeld*, 1982b]. In the $NH_4^+/NO_3^-/SO_4^{2-}$ mixture, additional $(NH_4)_2SO_4$ reduces the equilibrium constant, makes the aqueous system a more favorable medium for NH_4NO_3 formation, and shifts the thermodynamic equilibrium toward the aerosol phase.

For example, during a high RH (75.24 ± 10.63 %) period between the evening of 22 June and the morning of 23 June, 2011, RH was well above DRH. Nitrate reached the maximum value (0.84 μg m^{-3}) over the entire campaign, and the mean value during this time was 0.64 μg m^{-3} (~five times larger than the campaign-average value of 0.12 μg m^{-3}). The Pearson's correlation coefficient between NO_3^- and SO_4^{2-} during this period was 0.55 (an increase of ~70% compared to the campaign-wide r value of 0.32), indicating that NH_4NO_3 might be formed on the moist surface of pre-existing sulfate aerosols. Additionally, regression yields a good relationship between NO_3^- and particle surface area concentration measured by SEMS (r=0.71), indicating potential nitrate formation through heterogeneous conversion on particle surfaces. Similarly, during another high RH (72.66 ± 6.56 %) period

between the evening of 23 June and the morning of 24 June, 2011, NO_3^- increased to 0.54 μg m^{-3} and was strongly correlated with SO_4^{2-} (r=0.93). This further demonstrates that co-existence of SO_4^{2-} in the deliquescent aerosols favors aqueous NH_4NO_3 formation.

In Shanghai, *Pathak et al*. [2009] attributed high NO_3^- levels to the nighttime heterogeneous hydrolysis of dinitrogen pentoxide on the surface of SO_4^{2-} aerosols in an NH_3-deficient atmosphere. In Beijing, *Ianniello et al.* [2011] observed a strong relationship between NO_3^- and SO_4^{2-} (r=0.89) at high RH and estimated an average Y value of 0.2 with elevated NO_3^- concentrations during summertime. In Guangzhou, *Hu et al*. [2008] found that when RH is above DRH, $P_{NH3}P_{HNO3}$ is larger than the calculated K_{NH4NO3}^* and suggested that NH_4NO_3 formation is possible. All these studies interpreted the observations as nitrate being produced on the wet surface of pre-existing sulfate aerosols, underscoring the conclusion that the same process is important in this study area.

Measured particle number size distributions, given in Figure 6, display a growth in particle size between the evening of 23 June and the morning of 24 June, 2011, implying that NH_3 participated in an aerosol growth event as a result of the formation of aqueous NH_4NO_3 and $(NH_4)_2SO_4$ during that humid period. Meanwhile, both NH_4^+ and SO_4^{2-} reached their maximum values (2.03 μg m^{-3} and 5.84 μg m^{-3}, respectively) over the entire campaign, and the mean event values were 1.42 μg m^{-3} (~three times larger than the campaign-average value of 0.44 μg m^{-3} for NH_4^+) and 3.99 μg m^{-3} (~three times larger than the campaign-average value of 1.25 μg m^{-3} for SO_4^{2-}), respectively. Highly efficient gas-particle conversion contributed significantly to this specific pollution episode characterized by the highest PM_1 level observed in this study. Figure 7 shows a large increase in the size-resolved particle

number concentration during the event compared to the campaign-average size distribution. It can be seen that smaller particles (d_p < 250 nm) were major contributors to the episode. The ternary plot of NH_4^+, NO_3^-, and SO_4^{2-} shown in Figure 8 indicates the higher relative NO_3^- fraction at higher RH (percentage of concentrations in μeq m^{-3}). The proportion of NO_3^- in the inorganic components of PM_1 increased up to 21% compared with the campaign-average value of 4%, probably due to aqueous NH_4NO_3 formation.

It should be noted that no relationship was found between the observed NH_3 mixing ratios and the total particle number concentration measured by the SEMS, despite isolated events such as those depicted in Figure 6. Such a relationship has been simulated in power plant plumes in Houston [*Gong et al.*, 2013b]. The lack of such a relationship in the present study indicates the location of the sampling site far downwind from major emissions sources or that decreased gas-phase mixing ratios inhibited particle nucleation events that would increase particle number concentrations significantly.

Figure 4 (b) shows the theoretically calculated equilibrium constant for solid NH_4Cl (solid line) based on Equation (2) and the partial pressure product $P_{NH3}P_{HCl}$ as a function of ambient temperature under RH<DRH conditions. It can be seen that $P_{NH3}P_{HCl}$ calculated using measured mixing ratios of NH_3 and HCl was always smaller than K_{NH4Cl}. Therefore, the thermodynamic conditions were not favorable for NH_4Cl formation, and solid NH_4Cl is not expected to be formed at equilibrium, as with NH_4NO_3. Nevertheless, detailed investigations about the formation of solid and/or aqueous NH_4Cl are impeded by the unavailability of particulate chloride (Cl^-) data because Cl^- levels were at or near the detection levels of the HR-ToF-AMS and other high time-resolution instrumentation.

In the present work, the average gas fraction of NH_3 ($=NH_3/(NH_3+NH_4^+)$) is 0.76 ± 0.15, indicating that NH_3 remained predominantly in the gas phase rather than the aerosol phase. Additionally, the HNO_3 gas fraction ($=HNO_3/(HNO_3+NO_3^-)$), with a mean of 0.86 ± 0.10, reflects the lack of nitrate aerosol formation during most of the study period. High temperatures (30.15 ± 4.12 ^oC) favored the evaporation of volatile ammonium salts (e.g., NH_4NO_3 and NH_4Cl) and shifted the thermodynamic equilibrium toward the gas phase. Similar observations have been reported by other studies. *Robarge et al*. [2002] estimated an average gas fraction higher than 0.8 for NH_3 in summer at an agricultural site in the Coastal Plain region of North Carolina. *Saylor et al*. [2010] found much greater NH_3 levels compared to NH_4^+ in $PM_{2.5}$ in a rural area near Atlanta, leading to a mean NH_3 gas fraction of 0.89. *Baek and Aneja* [2004] measured ammonium-poor (1.64 ± 1.26 μg m^{-3}) aerosols in eastern North Carolina, while NH_3 (17.89 ± 15.03 μg m^{-3}) was abundant in the gas phase.

Ammonia preferentially reacts with H_2SO_4 in the atmosphere, and if extra NH_3 is available after the neutralization process, HNO_3 and HCl will further react with it. Here, excess NH_4^+ is defined as $[NH_4^+]$-$2[SO_4^{2-}]$ (in units of μmol m^{-3}). Figure 9 is an example of the relationship between excess NH_4^+ and NO_3^- during the event described previously. The slope (0.84) of the regression line and a Pearson's correlation coefficient of 0.94 suggest that NH_4NO_3 was formed. Analogously, *Du et al*. [2010] observed that the slope of the regression function between non-sulfate NH_4^+ and NO_3^- was 0.88 in the early summer at an urban site in Shanghai. The slope was further improved to 0.98 when Cl^- was included in the calculation. Thus, sufficient availability of NH_3 in the gas phase is indispensable for the complete neutralization with H_2SO_4 and for an environmental condition favoring HNO_3

partitioning into the aerosol phase.

3.3 Particulate Organic Nitrogen Formation

It is known that atmospheric NH_3 can react with gas-phase organic acids and organic aerosols to form condensable salts [*Na et al.*, 2003; *Kuwata and Martin*, 2012] and brown carbon [*Updyke et al.*, 2012], respectively. Figure 10 shows time series of HR-ToF-AMS nitrogen-containing organic fragments (CHN, CHON, and CHOgt1N, where gt1 implies more than one oxygen atom) during the previously defined event and the periods just before and just after the event. It can be seen that the mass concentration of organic nitrogen was elevated substantially during the humid period coincident with the aerosol growth event. The mean organic nitrogen concentration during the event period was 0.87 μg m^{-3} (~five times larger than the campaign-average value of 0.17 μg m^{-3}, which itself is skewed considerably by the event), indicating that significant NH_3-induced formation of organic nitrogen might have contributed to the increased particle concentrations at high RH via NH_3 reacting with gas-phase organic acids or partitioning into aqueous aerosols containing organic acids. It is also possible that the observed organic nitrogen resulted from other chemistry, such as that involving VOCs and NO_2 [*Jacobson*, 1999].

Organic nitrogen species are believed to contribute to light absorption. Although direct particle absorption measurements were not made during the campaign, an aethalometer was used to measure BC. Therefore, BC data during this event were investigated. The average concentration of BC was 0.45 μg C m^{-3} during the event (an increase of ~30% compared to the campaign-average value of 0.35 μg C m^{-3}); meanwhile CO levels also were significantly

elevated. As a consequence, the ratio of BC to CO did not increase substantially during the event compared to other measurement periods, suggesting the enhancement in BC is likely due to emissions from local fuel combustion sources, not from the formation of organic nitrogen. If organic nitrogen did contribute to light absorption during this event, it was likely at wavelengths other than those utilized by the aethalometer.

4. Conclusions

Comprehensive aerosol measurements were made northwest of Fort Worth in the early summer of 2011 (9 June– 30 June) using a HR-ToF-AMS, an aethalometer, and a SEMS simultaneously. When analyzed in conjunction with trace gas mixing ratios measured simultaneously, the impact of NH_3 on particle mass concentrations in the DFW atmosphere were investigated. Mass concentrations of aerosol species in sampled PM_1 showed a large amount of variability: SO_4^{2-} (1.25 ± 0.66 μg m^{-3}), NH_4^+ (0.44 ± 0.24 μg m^{-3}), and NO_3^- (0.12 ± 0.11 μg m^{-3}). Pearson's correlation coefficients between NH_4^+, SO_4^{2-}, and NO_3^- suggest that particulate NH_4^+ mainly existed as $(NH_4)_2SO_4$ and NH_4HSO_4 and that NH_4NO_3 was not formed during most of the study period, likely due to high temperatures (30.15 ± 4.12 ^oC) over the entire campaign. Ambient aerosols were nearly neutral.

In order to investigate the formation of NH_4NO_3 and NH_4Cl, theoretical calculations of thermodynamic equilibrium were performed. When RH<DRH, $P_{NH3}P_{HNO3}$ and $P_{NH3}P_{HCl}$ were always smaller than the estimated equilibrium constants K_{NH4NO3} and K_{NH4Cl}, indicating the absence of NH_4NO_3 and NH_4Cl formation. When RH>DRH, however, relatively increased levels of NO_3^- were observed. The strong relationships between NO_3^- and SO_4^{2-}

and surface area at high RH imply that NH_4NO_3 is formed on the moist surface of pre-existing sulfate aerosols. The co-existence of SO_4^{2-} in the wet particles lowers the equilibrium constant, providing a thermodynamically favorable condition for aqueous NH_4NO_3 formation. In addition, measured particle number size distributions clearly showed the occurrence of an aerosol growth event synchronous with ammonium salt formation during some humid periods characterized by increased concentrations of particulate NH_4^+, NO_3^-, and SO_4^{2-}. Excess NH_4^+ also was found to be closely correlated with NO_3^- during this event when PM_1 levels were significantly elevated. The significant NH_3-induced formation of organic nitrogen also might have contributed to the increased particle mass concentration at high RH. Extensive measurements in the future are desirable to better evaluate the effect of NH_3 on local and regional air quality with respect to PM formation in the DFW area, especially in winter, as NH_4NO_3 and NH_4Cl formation is much more favored under colder conditions.

Acknowledgements

This study was supported by the Mid-InfraRed Technologies for Health and the Environment (MIRTHE) Center and National Science Foundation (NSF) under grant No. EEC-0540832 and the TCEQ Air Quality Research Program. Support of A. P. Rutter by the Dreyfus Foundation is gratefully acknowledged. The authors would like to thank Melanie Calzada and Caroline Gutierrez for their help in data collection in the field and the Texas National Guard for providing access to the Eagle Mountain Lake site.

Reference

Baek, B. H., and V. P. Aneja (2004), Measurement and analysis of the relationship between ammonia, acid gases, and fine particles in eastern North Carolina, *J. Air & Waste Manage. Assoc.*, 54, 623-633.

Clarisse, L., C. Clerbaux, F. Dentener, D. Hurtmans, and P. Coheur (2009), Global ammonia distribution derived from satellite observations, *Nat. Geosci.*, *2*, 479-483.

Du, H., L. Kong, T. Cheng, J. Chen, X. Yang, R. Zhang, Z. Han, Z. Yan, and Y. Ma (2010), Insights into ammonium particle-to-gas conversion: non-sulfate ammonium coupling with nitrate and chloride, *Aerosol. Air Qual. Res.*, 10, 589-595.

Ellis, R. A., J. G. Murphy, M. Z. Markovic, T. C. VandenBoer, P. A. Makar, J. Brook, and C. Mihele (2011), The influence of gas-particle partitioning and surface-atmosphere exchange on ammonia during BAQS-Met, *Atmos. Chem. Phys.*, 11, 133-145.

Gong, L., R. Lewicki, R. J. Griffin, J. H. Flynn, B. L. Lefer, and F. K. Tittel (2011), Atmospheric ammonia measurements in Houston, TX using an external-cavity quantum cascade laser-based sensor, *Atmos. Chem. Phys.*, *11*, 9721–9733, doi:10.5194/acp-11-9721-2011.

Gong, L., R. Lewicki, B. Karakurt Cevik, A. P. Rutter, R. J. Griffin, F. K. Tittel, J. H. Flynn, B. L. Lefer, E. Scheuer, J. E. Dibb, and S. Kim (2013a), Characterization of atmospheric ammonia near Fort Worth, TX – Part I. Dynamics of gaseous ammonia, submitted to *J. Geophys. Res.*

Gong, L., R. Lewicki, R. J. Griffin, F. K. Tittel, C. R. Lonsdale, R. G. Stevens, J. R. Pierce, Q. G. J. Malloy, S. A. Travis, L. M. Bobmanuel, B. L. Lefer, and J. H. Flynn (2013b), Role of atmospheric ammonia in particulate matter formation in Houston during summertime, *Atmos. Environ.*, in press.

Hu, M., Z. Wu, J. Slanina, P. Lin, S. Liu, and L. Zeng (2008), Acidic gases, ammonia and water-soluble ions in $PM_{2.5}$ at a coastal site in the Pearl River Delta, China, *Atmos. Environ.*, 42, 6310-6320.

Ianniello, A., F. Spataro, G. Esposito, I. Allegrini, M. Hu, and T. Zhu (2011), Chemical characteristics of inorganic ammonium salts in $PM_{2.5}$ in the atmosphere of Beijing (China), *Atmos. Chem. Phys.*, 11, 10803-10822.

IPCC (2007), Climate Change 2007. Synthesis Report. Contribution of Working Groups I, II and III to the Fourth Assessment Report of the Intergovernmental Panel on Climate Change [Core Writing Team, Pachauri, R. K. and Reisinger, A. (eds.)]. *IPCC*, Geneva, Switzerland, 104 pp.

Jacobson, M. Z. (1999), Isolating nitrated and aromatic aerosols and nitraed aromatic gases as sources of ultraviolet light absorption, *J. Geophys. Res.*, 104, 3527-3542.

Kuwata, M., and S. T. Martin (2012), Phase of atmospheric secondary organic material affects its reactivity, *Proc. Natl. Acad. Sci.*, 109, 17354-17359.

Meng, Z. Y., W. L. Lin, X. M. Jiang, P. Yan, Y. Wang, Y. M. Zhang, X. F. Jia, and X. L. Yu (2011), Characteristics of atmospheric ammonia over Beijing, China, *Atmos. Chem. Phys.*, 11, 6139-6151.

Myles, L. (2009), Atmospheric science: Underestimating ammonia, *Nat. Geosci.*, *2*, 461-462.

Na, K., C. Song, and D. Cocker (2007), Effect of ammonia on secondary organic aerosol

formation from α-pinene ozonolysis in dry and humid conditions, *Environ. Sci. Technol.*, 41, 6096-6102.

Nowak, J. B., J. A. Neuman, R. Bahreini, A. M. Middlebrook, J. S. Holloway, S. A. McKeen, D. D. Parrish, T. B. Ryerson, and M. Trainer (2012), Ammonia sources in the California South Coast Air Basin and their impact on ammonium nitrate formation, *Geophys. Res. Lett.*, 39, L07804, doi:10.1029/2012GL051197.

Pandolfi, M., F. Amato, C. Reche, A. Alastuey, R. P. Otjes, M. J. Blom, and X. Querol (2012), Summer ammonia measurements in a densely populated Mediterranean city, *Atmos. Chem. Phys.*, 12, 7557-7575.

Pathak, R. K., W. S. Wu, and T. Wang (2009), Summertime $PM_{2.5}$ ionic species in four major cities of China: nitrate formation in an ammonia-deficient atmosphere, *Atmos. Chem. Phys.*, 9, 1711-1722.

Pio, C. A., and R. M. Harrison (1987), The equilibrium of ammonium chloride aerosol with gaseous hydrochloric acid and ammonia under tropospheric conditions, *Atmos. Environ.*, 21, 1243-1246.

Pope, C. A., and D. W. Dockery (2006), Health effects of the fine particulate air pollution: lines that connect. *J. Air & Waste Manage. Assoc.*, 56, 709–774.

Robarge, W. P., J. T. Walker, R. B. McCulloch, and G. Murray (2002), Atmospheric concentrations of ammonia and ammonium at an agricultural site in the southeast United States, *Atmos. Environ.*, 36, 1661-1674.

Sarwar, G., R. L. Corsi, K. A. Kinney, J. A. Banks, V. M. Torres, and C. Schmidt (2005), Measurements of ammonia emissions from oak and pine forests and development of a non-industrial ammonia emissions inventory in Texas, *Atmos. Environ.*, 39, 7137-7153.

Saylor, R. D., E. S. Edgerton, B. E. Hartsell, K. Baumann, and D. A. Hansen (2010), Continuous gaseous and total ammonia measurements from the southeastern aerosol research and characterization (SEARCH) study, *Atmos. Environ.*, 44, 4994-5004.

Seinfeld, J. H., and S. N. Pandis (2006), Atmospheric Chemistry and Physics: From Air Pollution to Climate Change, *John Wiley*, New York.

Stanier, C. O., A. Singh, W. Adamski, J. Baek, M. Caughey, G. Carmichael, E. Edgerton, D. Kenski, M. Koerber, J. Oleson, T. Rohlf, S. R. Lee, N. Riemer, S. Shaw, S. Sousan, and S. N. Spak (2012), Overview of the LADCO winter nitrate study: hourly ammonia, nitric acid and $PM_{2.5}$ composition at an urban and rural site pair during $PM_{2.5}$ episodes in the US Great Lakes region, *Atmos. Chem. Phys. Discuss.*. 12, 14115-14167.

Stelson, A. W. (1982), Thermodynamics of aqueous atmospheric aerosols. Dissertation (Ph.D.), California Institute of Technology.

Stelson, A. W., and J. H. Seinfeld (1982a), Relative humidity and temperature dependence of the ammonium nitrate dissociation constant, *Atmos. Environ.*, 16, 983-992

Stelson, A. W., and J. H. Seinfeld (1982b), Thermodynamic prediction of the water activity, HN_4NO_3 dissociation constant, density and refractive index for the NH_4NO_3-$(NH_4)_2SO_4$-H_2O system at 25 ^oC, *Atmos. Environ.*, 16, 2507-2514.

Sutton, M. A., J. W. Erisman, F. Dentener, and D. Möller (2008), Ammonia in the environment: From ancient times to the present, *Environ. Pollut.*, *156*, 583-604.

Updyke, K. M., T. B. Nguyen, and S. A. Nizkorodov (2012), Formation of brown carbon via reactions of ammonia with secondary organic aerosols from biogenic and anthropogenic

precursors, *Atmos. Environ.*, 63, 22-31.
U.S. EPA (2008), National Emissions Inventory (NEI) Data Version 2, http://www.epa.gov/ttn/chief/net/2008inventory.html.

Table 1. Statistics of inorganic aerosol components in PM_1 (μg m^{-3}) collected during the measurement period.

	SO_4^{2-}	NO_3^-	NH_4^+
Mean	1.25	0.12	0.44
Standard Deviation	0.66	0.11	0.24
Maximum	5.84	0.84	2.03
Minimum	0.20	0.03	0.06
Median	1.09	0.09	0.39
10th Percentile	0.62	0.06	0.21
25th Percentile	0.81	0.07	0.27
75th Percentile	1.57	0.13	0.56
90th Percentile	2.09	0.19	0.74

List of figures

Figure 1. Time series of hourly-averaged HR-ToF-AMS data along with meteorological parameters during the study period (9 June 2011 – 30 June 2011).

Figure 2. Diurnal profiles of (a) NH_4^+; (b) NO_3^-; and (c) SO_4^{2-} during the measurements.

Figure 3. Scatter plots of [NH_4^+] versus [NO_3^-], [SO_4^{2-}], and [NO_3^-] + 2[SO_4^{2-}] (in units of μmol m^{-3}) during sampling periods.

Figure 4. Theoretically calculated equilibrium constant (solid line) as a function of ambient temperature under RH<DRH conditions for (a) solid NH_4NO_3 based on Equation (1) and $P_{NH3}P_{HNO3}$ (black dots); and (b) solid NH_4Cl based on Equation (2) and $P_{NH3}P_{HCl}$ (black dots).

Figure 5. Scatter plot of [NO_3^-] versus [SO_4^{2-}] (in units of μg m^{-3}) color-coded by RH over the entire campaign.

Figure 6. Contour plot of particle number size distribution between 23 June and 25 June.

Figure 7. Size-resolved particle number concentration during the entire campaign and during the aerosol growth event.

Figure 8. Ternary plot of NH_4^+, NO_3^-, and SO_4^{2-} during the campaign.

Figure 9. Scatter plot of excess [NH_4^+] versus [NO_3^-] during the aerosol growth event.

Figure 10. Time series of hourly-averaged HR-ToF-AMS organic nitrogen fragments during a subset of the study period (19-29 June 2011).

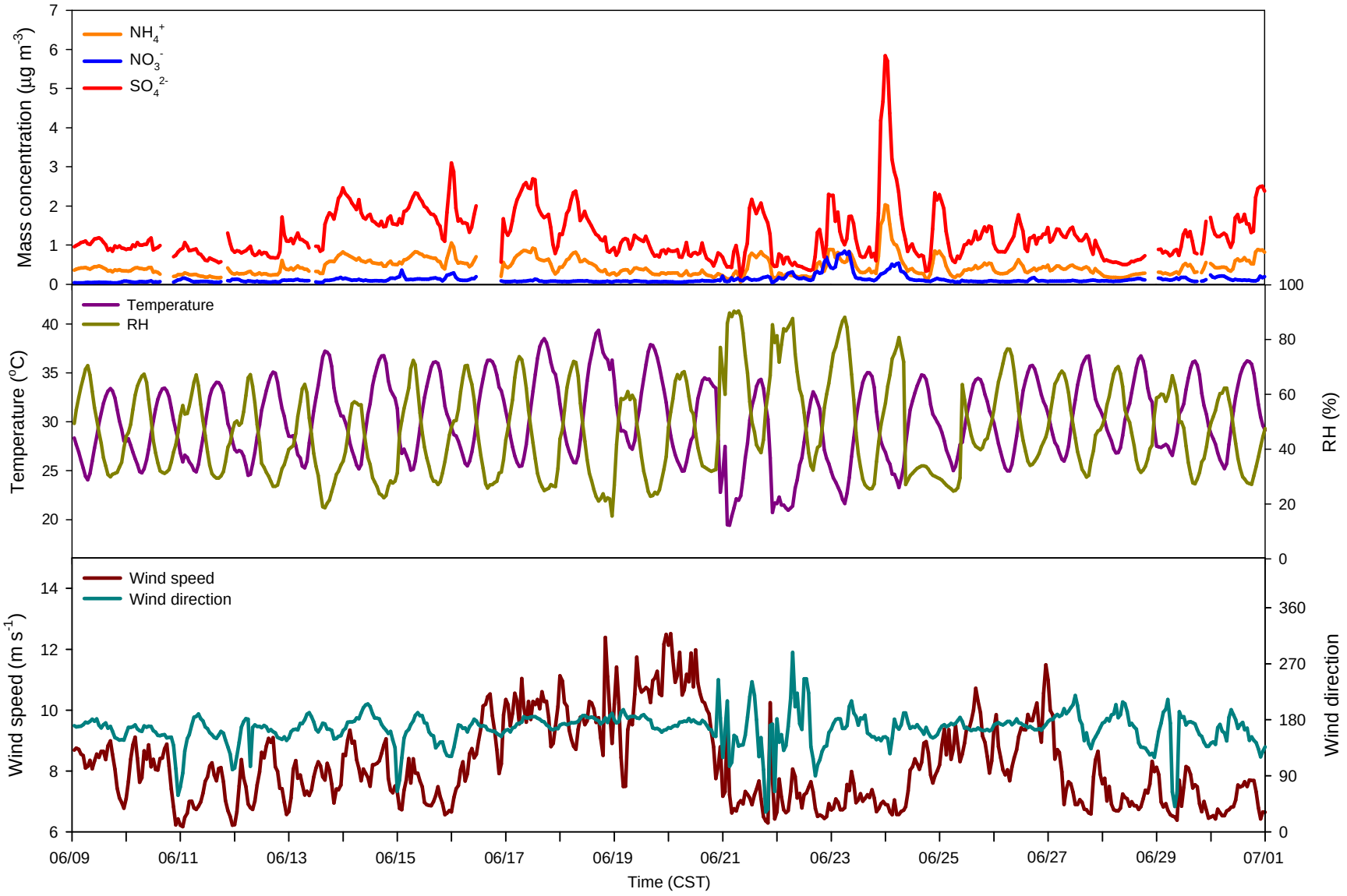
NH4+
NO3-
SO42-
Mass concentration (μg m-3)
Temperature
RH
Temperature (oC)
RH (%)
Wind speed
Wind direction
Wind speed (m s-1)
Wind direction
06/09
06/11
06/13
06/15
06/17
06/19
06/21
06/23
06/25
06/27
06/29
07/01
Time (CST)

Figure 1

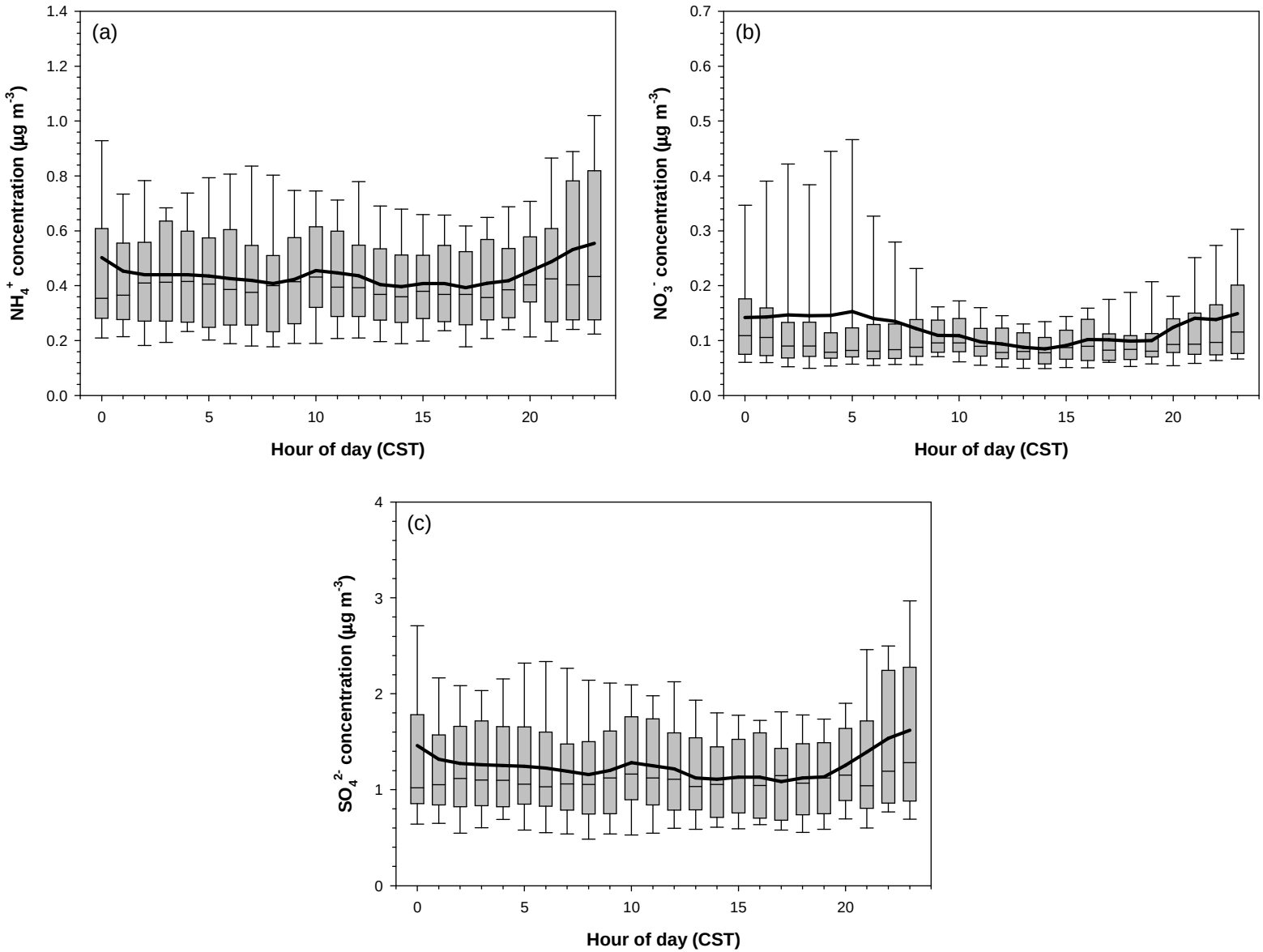
(a)
NH_4^+ concentration (μg m^{-3})
Hour of day (CST)
(b)
NO_3^- concentration (μg m^{-3})
Hour of day (CST)
(c)
SO_4^{2-} concentration (μg m^{-3})
Hour of day (CST)

Figure 2

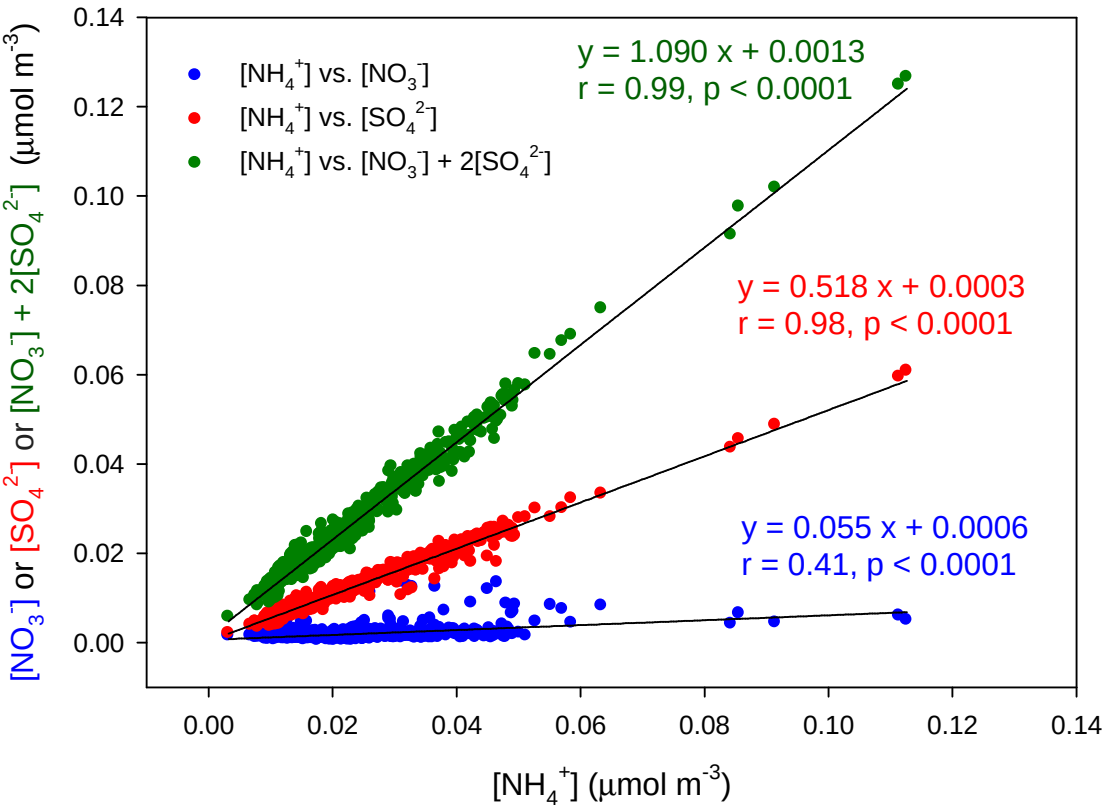
[NH4+] vs. [NO3-]
[NH4+] vs. [SO4 2-]
[NH4+] vs. [NO3-] + 2[SO4 2-]
y = 1.090 x + 0.0013
r = 0.99, p < 0.0001
y = 0.518 x + 0.0003
r = 0.98, p < 0.0001
y = 0.055 x + 0.0006
r = 0.41, p < 0.0001
[NO3-] or [SO4 2-] or [NO3-] + 2[SO4 2-] (µmol m-3)
[NH4+] (µmol m-3)
0.00
0.02
0.04
0.06
0.08
0.10
0.12
0.14

Figure 3

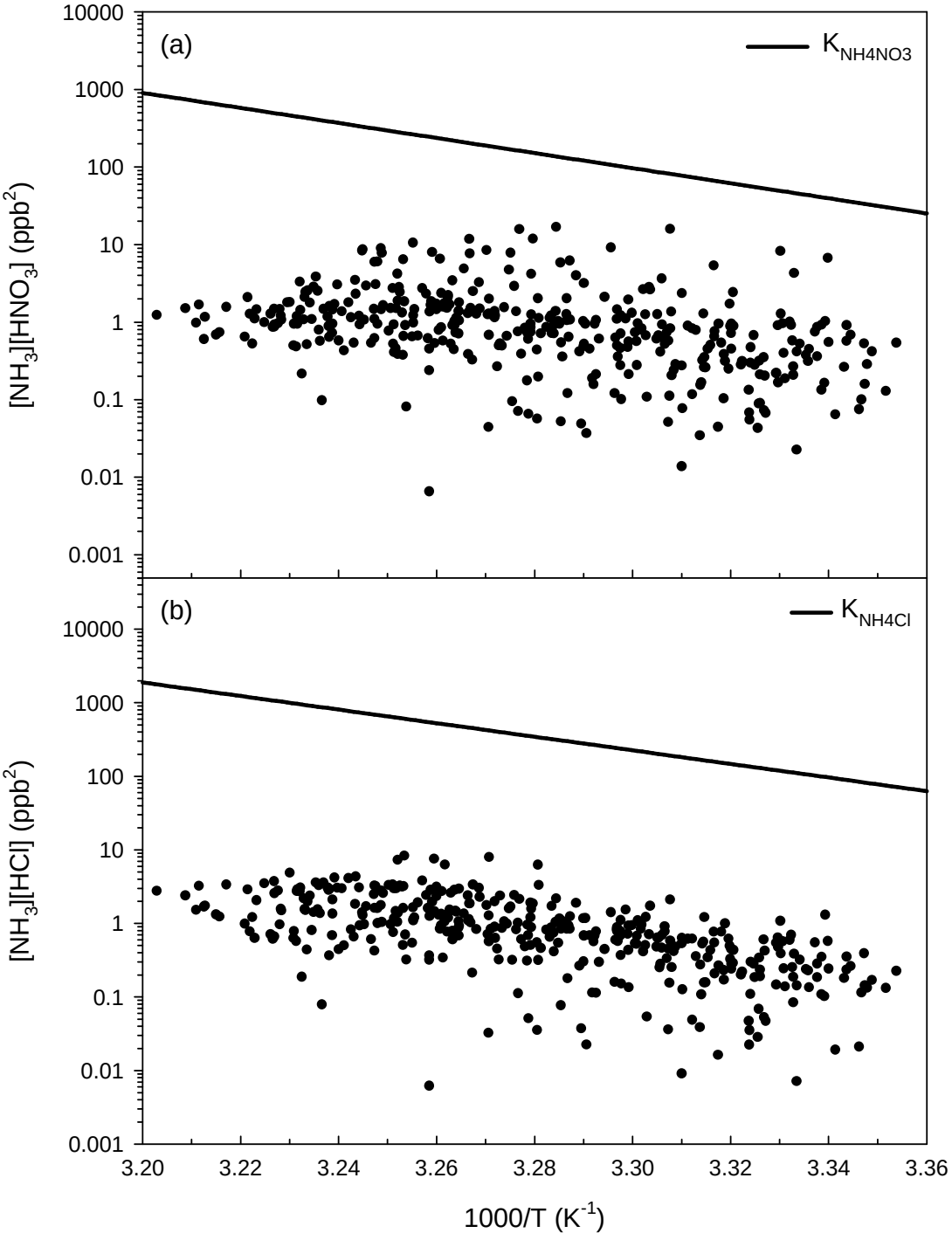
(a)
K_{NH4NO3}
$[NH_3][HNO_3]$ (ppb^2)
(b)
K_{NH4Cl}
$[NH_3][HCl]$ (ppb^2)
10000
1000
100
10
1
0.1
0.01
0.001
3.20
3.22
3.24
3.26
3.28
3.30
3.32
3.34
3.36
1000/T (K^{-1})

Figure 4

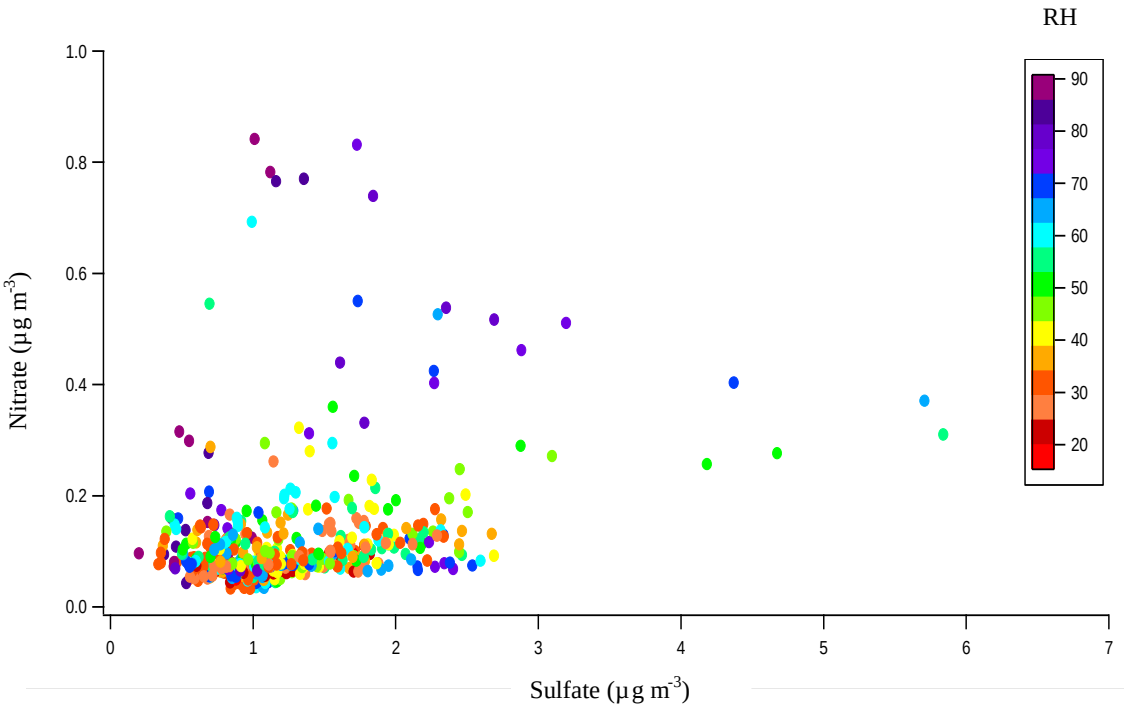
RH
90
80
70
60
50
40
30
20
1.0
0.8
0.6
0.4
0.2
0.0
Nitrate (µg m-3)
0
1
2
3
4
5
6
7
Sulfate (µg m-3)

Figure 5

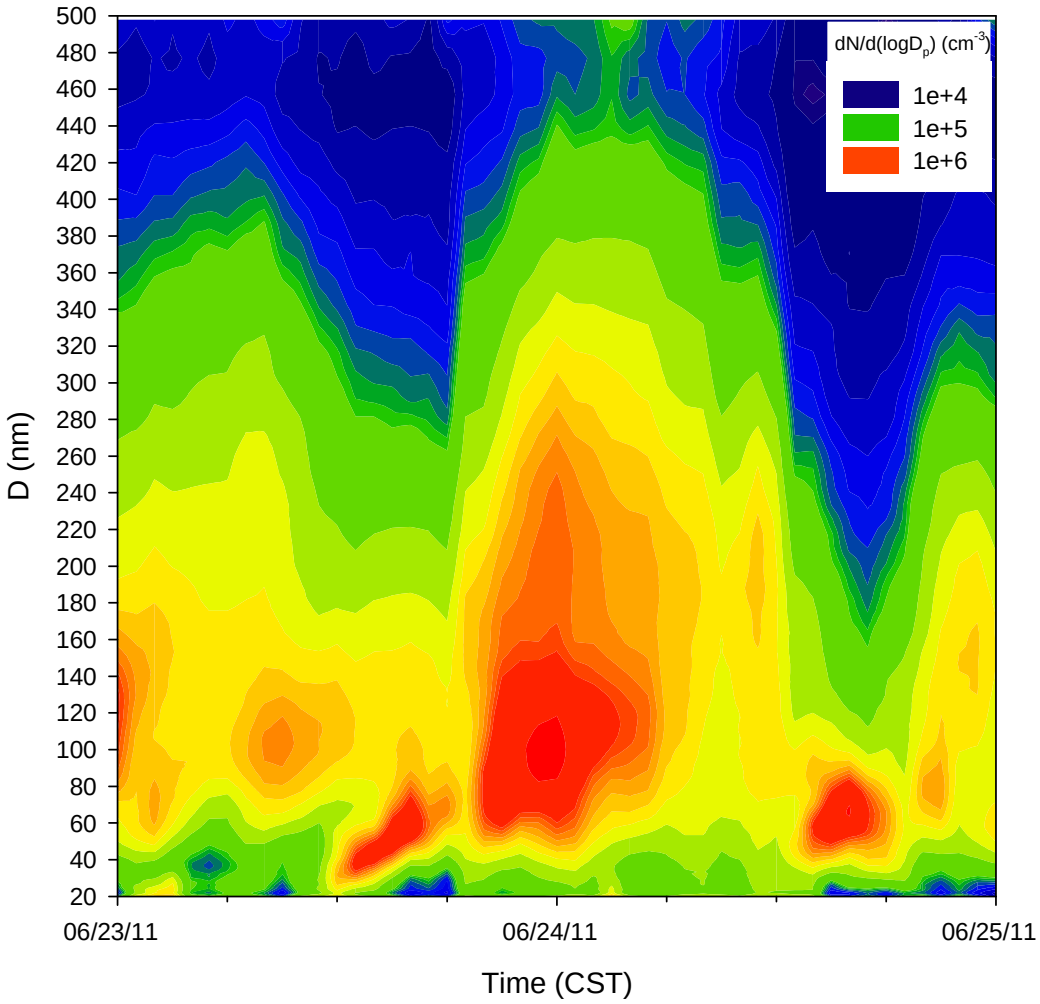
dN/d(logD$_p$) (cm^{-3})
1e+4
1e+5
1e+6
D (nm)
500
480
460
440
420
400
380
360
340
320
300
280
260
240
220
200
180
160
140
120
100
80
60
40
20
06/23/11
06/24/11
06/25/11
Time (CST)

Figure 6

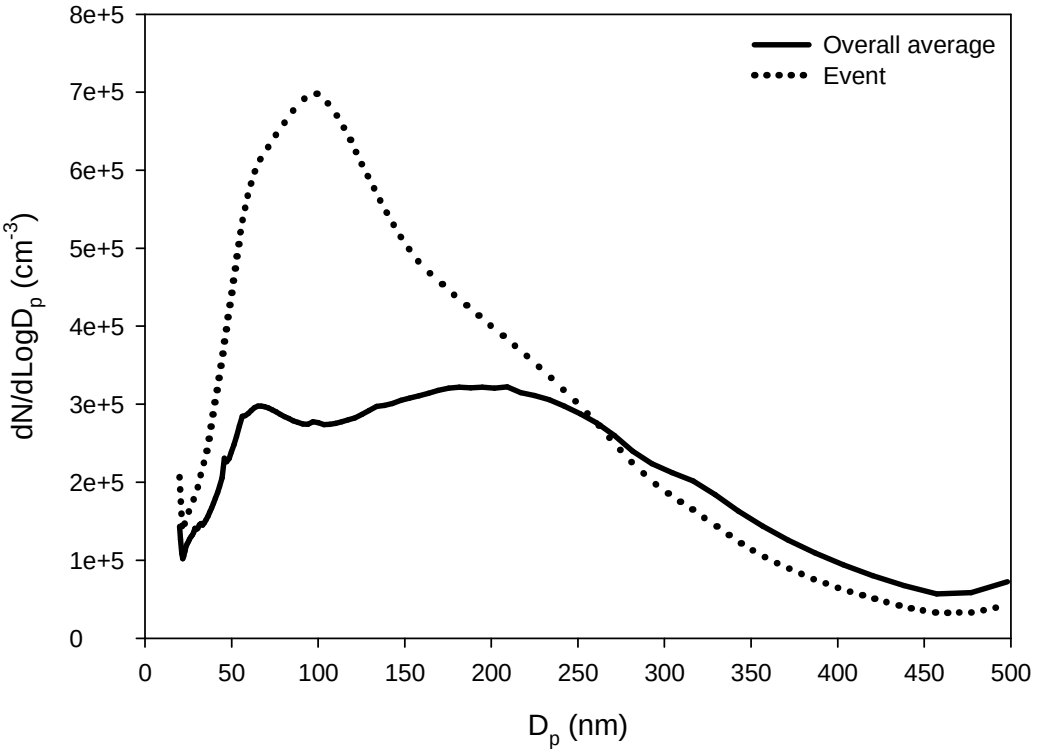
8e+5
7e+5
6e+5
5e+5
4e+5
3e+5
2e+5
1e+5
0
dN/dLogDp (cm-3)
0
50
100
150
200
250
300
350
400
450
500
Dp (nm)
Overall average
Event

Figure 7

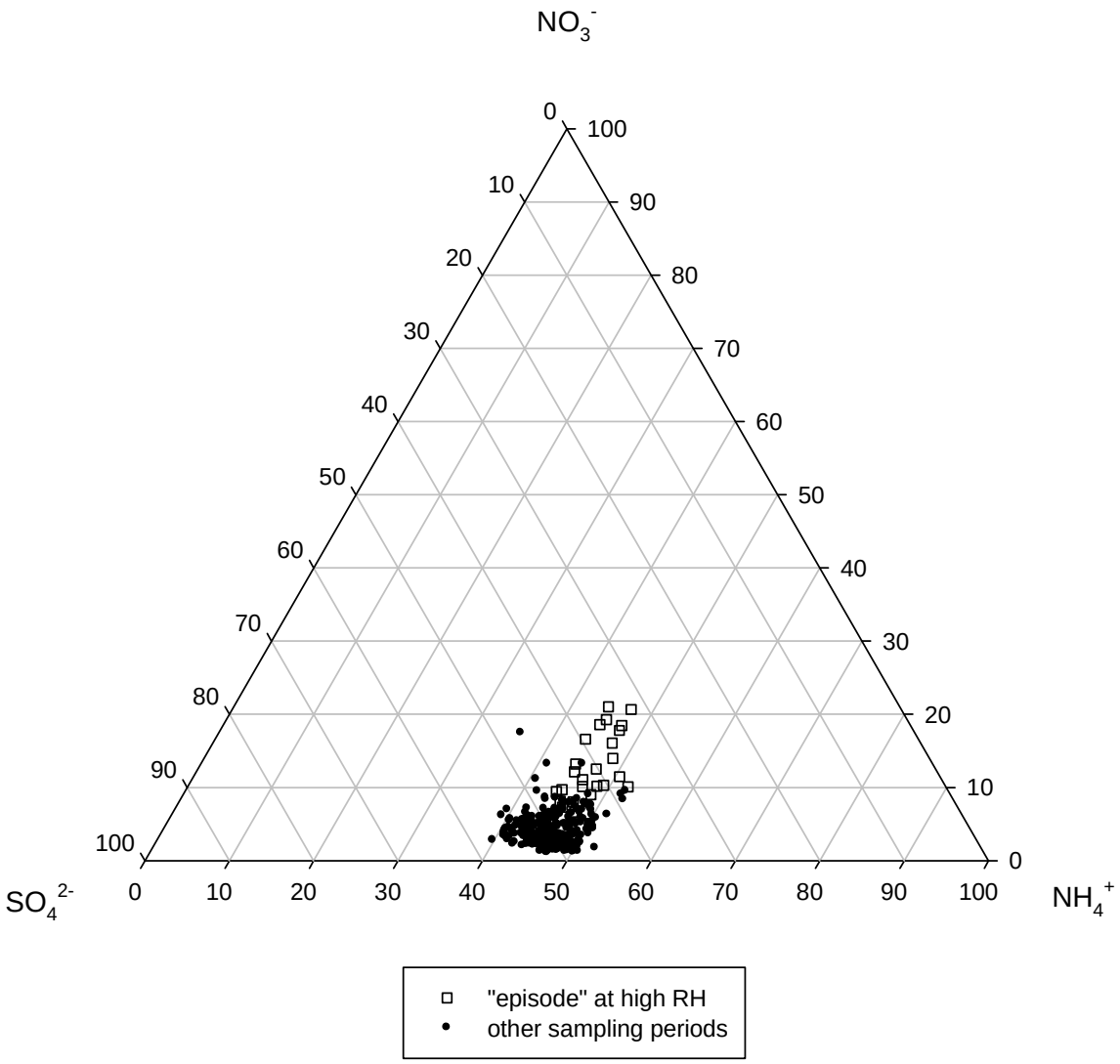
NO3-
0
100
10
90
20
80
30
70
40
60
50
50
60
40
70
30
80
20
90
10
100
0
SO4 2-
0 10 20 30 40 50 60 70 80 90 100
NH4+
"episode" at high RH
other sampling periods

Figure 8

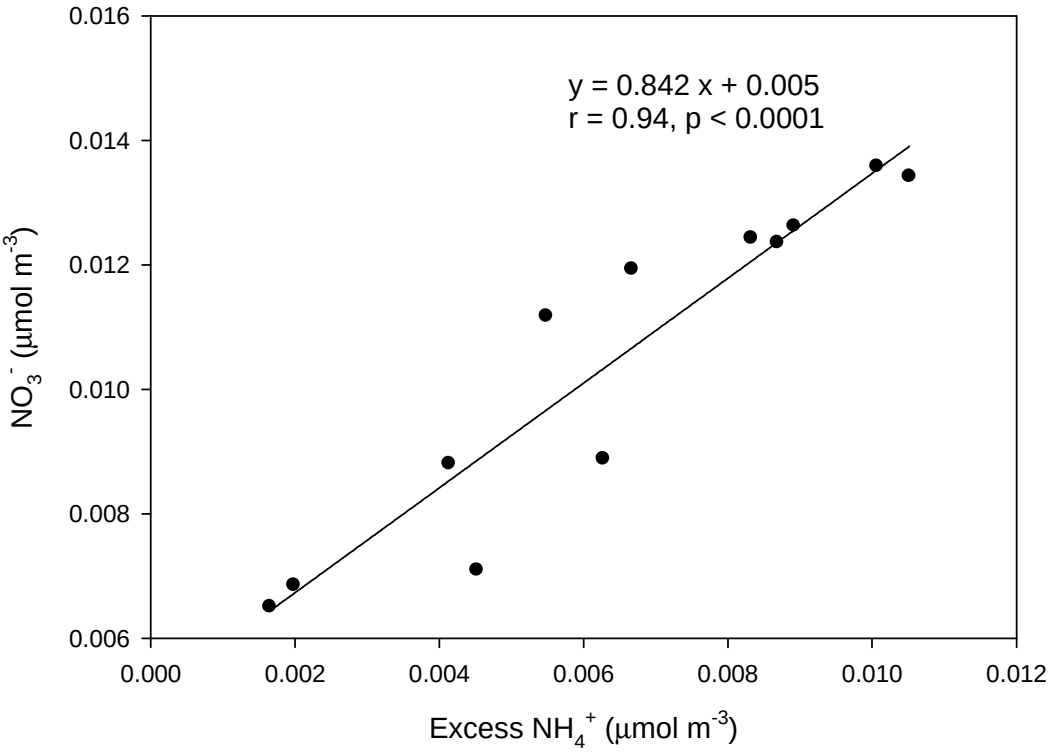
y = 0.842 x + 0.005
r = 0.94, p < 0.0001
0.016
0.014
0.012
0.010
0.008
0.006
0.000
0.002
0.004
0.006
0.008
0.010
0.012
NO3- (µmol m-3)
Excess NH4+ (µmol m-3)

Figure 9

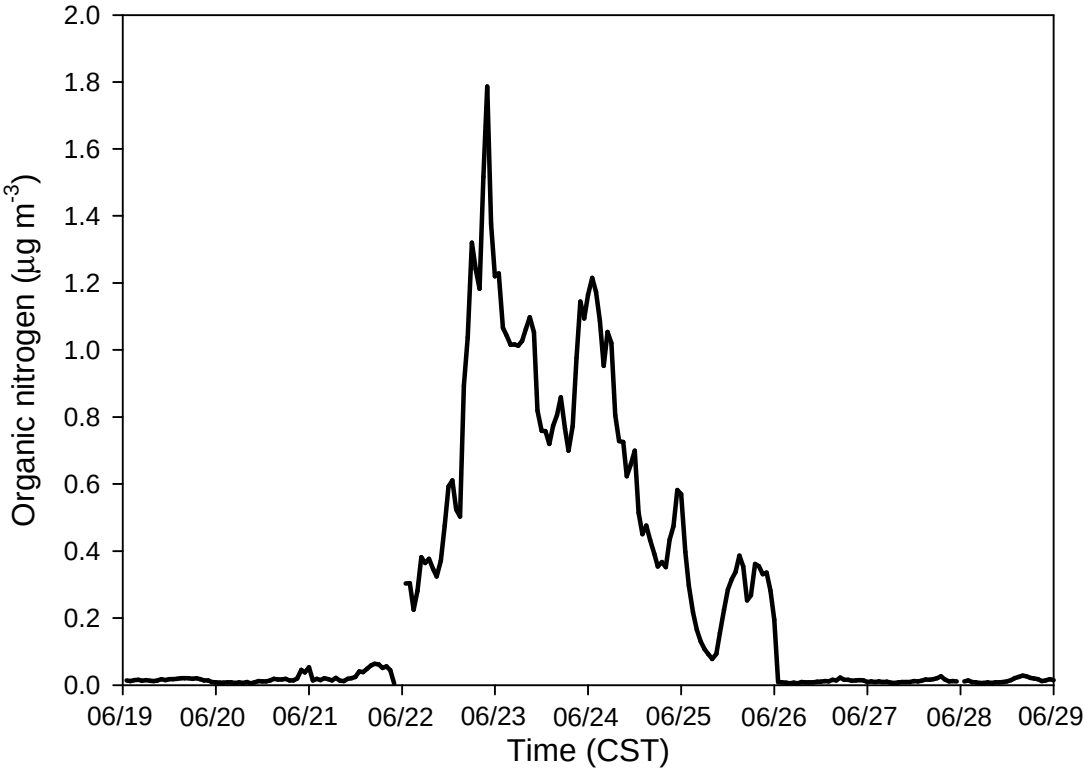
Organic nitrogen (µg m-3)
2.0
1.8
1.6
1.4
1.2
1.0
0.8
0.6
0.4
0.2
0.0
06/19
06/20
06/21
06/22
06/23
06/24
06/25
06/26
06/27
06/28
06/29
Time (CST)

Figure 10